Experimental and theoretical study of the elastic-electron–indium-atom scattering in the intermediate energy range

M. S. Rabasović,[1] V. I. Kelemen,[2] S. D. Tošić,[1] D. Šević,[1] M. M. Dovhanych,[2] V. Pejčev,[1,3] D. M. Filipović,[1,4] E. Yu. Remeta,[2] and B. P. Marinković[1]

[1]*Institute of Physics, Pregrevica 118, 11080 Belgrade, Serbia*

[2]*Institute of Electron Physics, National Academy of Sciences of Ukraine, Universitetska 21, Uzhgorod, Ukraine 88017*

[3]*Faculty of Natural Sciences, Kragujevac University, Radoja Domanovića 12, 34000 Kragujevac, Serbia*

[4]*Faculty of Physics, University of Belgrade, P.O. Box 368, 11001 Belgrade, Serbia*

(Received 19 November 2007; published 23 June 2008)

The results of experimental and theoretical studies on elastic-electron scattering by indium atom are presented. The measurements are performed at incident electron energies of E_0=10, 20, 40, 60, 80, and 100 eV within the scattering angles ranging from 10° to 150°. Theoretical calculations have been carried out using both complex and real optical potentials and cover the energy range up to E_0=350 eV. We report on relative differential cross sections (DCSs), integral (σ_{el}), momentum-transfer (σ_m), and viscosity (σ_v) cross sections for elastic-electron scattering. The energy dependence of the angular positions of DCS minima is also determined. Two data sets were calculated, with and withoutt an absorption potential being compared to the experimental results.

DOI: 10.1103/PhysRevA.77.062713 PACS number(s): 34.80.Bm, 31.15.E−

I. INTRODUCTION

Indium is a soft, gray metallic element which belongs to the elements of group III of the Periodic Table. It was found and spectroscopically identified as a minor component in zinc ores. Because of its low melting point, 429.75 K, it is technologically attractive especially in the semiconductor and optoelectronics. Its current primary application is in transparent electrodes made of indium tin oxide in liquid crystal displays (LCD). The spectral lines of neutral and ionized indium could be of interest in the determination of plasma parameters [1]. The solar indium abundance is also analyzed in the astrophysical investigations [2]. Another very important role of indium is the application of an indium single ion as a reference for an optical frequency standard of unprecedented stability and accuracy. In^+ is the only one with an alkaline-earth-like spectrum. A narrow transition of a laser—cooled ion, stored in the radio-frequency trap serves as the clock transition [3].

Indium atom is the first of a series of the 5*p* elements of the Periodic Table, which ends by xenon atom. The atoms of this series are characterized by the relatively small value of the dipole static polarizability α_d, ranging from 30.4 a_0^3 for In to 27.3 a_0^3 for Xe [4]. On the other hand, indium atom belongs to the metals. Recent experimental measurements and theoretical investigations of DCS for Ca [5] and Yb [6,7] atoms with large α_d values ($\sim$150 a_0^3) have demonstrated a considerable difference in the form of DCS angular dependence as compared to noble gases. For example, DCSs for the Ca atom have three minima at 10 eV and 20 eV and two minima at 40, 50, and 100 eV. In the case of the Yb atom at 80 eV no structure of the "minimum-maximum" type was noticed within the entire angular range, while at lower energies, i.e., at 10–60 eV, two minima were found.

In the present paper, we have carried out calculations using the complex phenomenological optical potential (OP) with allowance made for spin-orbit interaction. The real part of this potential without absorption is called below the SEPSo approximation. This approach contains no adjustable parameter, and consists of static, local exchange, polarization, and spin-orbit potentials. We used the McCarthy-type potential [8,9] as the imaginary part of OP, which takes into account the absorption effects (the SEPASo approximation). An adequate description of absorption (i.e., the possible energy loss) in the elastic-electron scattering by complex atoms is one of the most difficult tasks. This particularly relates to the atomic systems with close valence and subvalence subshells, where the role of so-called intershell correlations is important. Therefore, it is not surprising that the adjustable parameters are used in the model absorption potentials. We have used the experimental integral cross sections for In atom excitation from the ground state and the single ionization cross sections [10–12] to determine the phenomenological parameter in the collision energy range under study at 10–300 eV.

The relativistic effects in the target atom were taken into account due to the use of a local relativistic approximation of the density functional theory (DFT). In this approximation, we have calculated total and subshell electron densities of indium atom. Note that the potential components of OP are determined, to some extent, by the electron densities. Therefore, for investigation of the collisions of electrons with In atoms the analytical parametrized expressions for static potential, total and subshell ($4d^{10}$,$5s^2$, and 5*p*) electron densities were obtained.

The goal of this work is to compare the measured and calculated results on DCSs and integrated cross sections ($\sigma_{el}, \sigma_m, \sigma_v$) of elastic-electron scattering by the indium atom. No experimental electron-collision data existed on the In atom prior to our present measurements. DCSs have been measured using an electron spectroscopy technique in the 10°–150° angular range and at 10, 20, 40, 60, 80, and 100 eV collision energies. Also, we have made theoretical studies of DCSs and integrated cross sections at larger energies

(100–350 eV) and determined the positions of critical minima in the 10–350 eV range. The relative values of the measured DCSs are normalized to the present theoretical calculations with the allowance of absorption. These normalized DCSs were used to obtain the experimental integral elastic (σ_{el}), momentum-transfer (σ_m), and viscosity (σ_v) cross sections. Our preliminary data has been recently reported at the XXV ICPEAC [13].

In Sec. II, the experimental procedure is given. The description of the theoretical approach and calculation method are presented in Sec. III. The results are presented and discussed in Sec. IV, and, finally, a conclusion is given.

II. EXPERIMENTAL PROCEDURE

In the present study, we have employed an electron spectrometer in crossed electron-atom beam arrangement. This experimental setup is already used for experiments with Ca, Mg, and Pb atoms and it has been described elsewhere [5,14–16]. The apparatus consists of an oven for the production of an atomic beam, an electron monochromator, and analyzer. For our measurements we have used one of three different modes in which the spectrometer can be operated, i.e., recording angular distribution of elastically scattered electrons.

Indium vapor beam was produced by heating the oven crucible containing In metal (99.9% purity). The oven has been modified in order to achieve higher temperatures. The oven consists of two separate heaters with the same diameters, one for the top of the stainless steel crucible and nozzle, and the other for the body of the crucible, and their temperatures were controlled by two thermocouples. The heating currents of those heaters were 5.3 and 3.4 A, respectively. They provided a variable temperature difference between the top and the bottom. The nozzle was maintained at approximately 100° higher temperature. The atomic beam was effused through a 20 mm long channel in the cap of the oven crucible that has an inner diameter of 2.5 mm, so the aspect ratio was 0.125. Working temperature was approximately 1300 K and the metal-vapor pressure was about 10 Pa or (0.07 units of Torr). Water cooling of oven, insulation ceramics, as well as several tantalum shields protected the channel electron multiplier from overheating. The background pressure was of the order of 10^{-5} Pa.

The energy scale was calibrated by measuring the position of the feature in the energy dependence of elastic scattering, attributed to the threshold energy of the $^2S_{1/2}$ excitation of indium at 3.025 eV. The uncertainty of the energy scale is determined to be 100 meV, overall energy resolution of 120 meV, and the angular resolution was estimated to be 1.5°.

The position of the real zero scattering angle was determined before each run by checking the symmetry of the inelastically (excitation of the $^2S_{1/2}$ state) scattered electron distribution around the mechanical zero at positive and negative angles (from −10° to +10°). The associated error in the angular scale determination was ±0.2°. Measurements at 0° were not reliable due to two reasons: first, there was some access noise originating from primary beam electrons although the energy selection of the analyzer was very efficient; second, the present angular resolution was not sufficient to record the true intensity of strongly forward peaked angular distribution.

In the present work relative DCSs for the elastic scattering are obtained as follows. For a given incident energy E_0, the position of the analyzer was changed from 10° to 150° and the angular distribution of scattered electrons was measured. A channeltron was used for single electron counting. That angular distribution was converted into relative DCSs by using the appropriate effective length correction factor. We have applied the correction factors of Brinkmann and Trajmar [17], modified for our experimental conditions.

The total error for relative DCS values arises from statistical errors, angular scale uncertainty, energy scale uncertainty, and estimation of the applied effective path-length correction. The statistical error was less than 0.10 (except at the DCS minima where it was less than 0.40). The contribution to the error from the angular uncertainty is up to 0.06 for small scattering angles and high energies. The contribution of the uncertainty in the energy scale is determined to be less than 0.05. The contribution to the error from the geometrical effective path-length correction factor is estimated to be 0.06.

III. THEORY

A. Potentials

Similarly to Refs. [18,19], for the phenomenological optical potential with allowance of absorption we use the complex potential

$$V_{\mathrm{opt}}^{\pm}(r,E) = V_R^{\pm}(r,E) + iV_a(r,E) \tag{1}$$

as the SEPASo approximation. The calculation without absorption potential V_a, when only the real part of Eq. (1) is taken,

$$V_R^{\pm}(r,E) = V_s(r) + V_e(r,E) + V_p(r) + V_{\mathrm{so}}^{\pm}(r), \tag{2}$$

is called the SEPSo approximation. The terms V_s, V_e, V_p, and V_{so} in Eqs. (1) and (2) are the static, exchange, polarization, and spin-orbit potentials, respectively. The notation "±" implies the values of total angular momentum of electron $j = \ell \pm 1/2$, ℓ being the electron orbital momentum. Here we use the atomic unit system (a.u.): $\hbar = e = m_e = 1$, $E = k^2/2$ is the energy, and k is the momentum of the incident electron.

Electron density $\rho(r)$ of indium atom was calculated within the framework of the local scalar-relativistic approximation of DFT with the exclusion of electron self-action energy (see, e.g., Sec. 2.2 in Ref. [19], and references therein). As a result of the least-square approximation of the initial tabulated data for the total electron density, the best approximation was obtained with the use of the analytical expression taken from Ref. [20] [see Eq. (A1) in Appendix A]. The static potential $V_s(r)$ is calculated by the analytical expression Eq. (A2) and, as well as in Ref. [20], is related to the expression for $\rho(r)$. Expressions for $\rho(r)$ and $V_s(r)$ used here are somehow more complex than the analytical expressions from Ref. [21] [Eqs. (11) and (12)] for approximation of the data obtained in the Dirac-Hartree-Fock-Slater approxima-

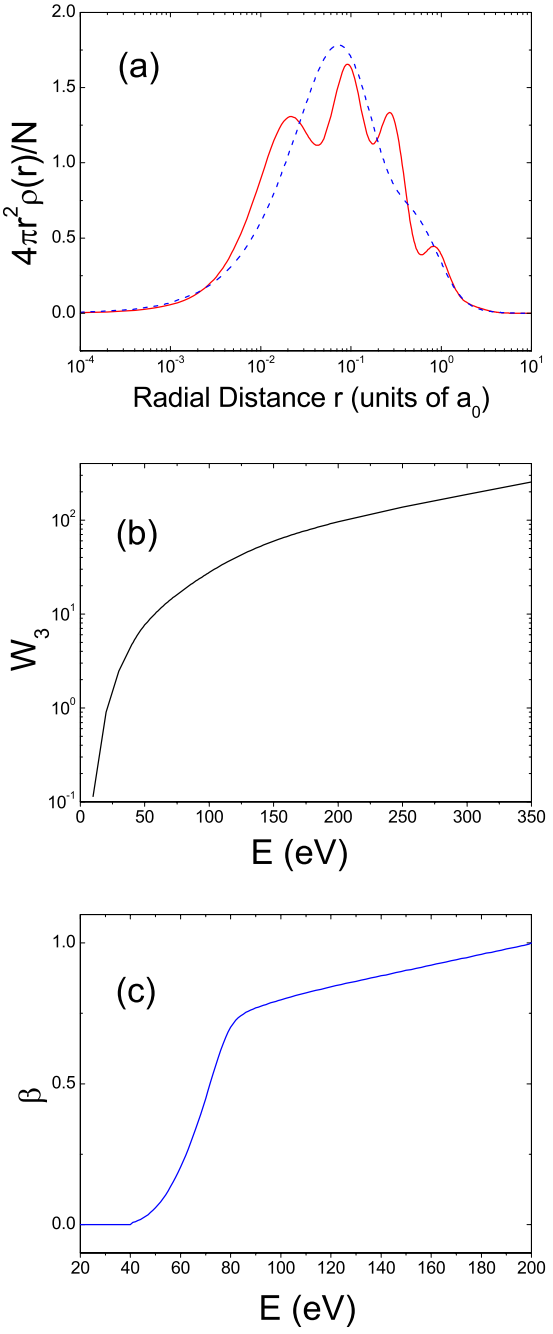

FIG. 1. (Color online) (a) Radial electron density $4\pi r^2\rho(r)/N$ in indium atom reduced to electron number $N=49$. The solid line is the calculation with $\rho(r)$ from Eq. (A1) and the dashed line is $\rho(r)$ taken from Ref. [21] [Eq. (12)]. (b) Energy dependence of parameters $W_3(E)$ for absorption potential $VA_3(r,E)$. (c) Energy dependence of parameters $\beta(E)$ for absorption potential $VA_3(r,E)$.

tion. In particular, $V_s(r)$ in Ref. [21] [Eq. (11)] is a simple superposition of three Yukawa-type potentials. However, as seen in Fig. 1(a), the use of the approximation Eq. (A1), unlike Ref. [21], reproduces a complex electron shell structure of indium atom.

The local potential in the free electron gas (FEG) approximation was taken as the exchange potential $V_e(r,E)$ in Ref. [22] [see also Eq. (2) in Ref. [19]]. The ionization potential for indium atom necessary for V_e calculation is $I=5.7864$ eV [23].

As the polarization potential $V_p(r)$ in Eq. (2) we use the correlation-polarization potential suggested in Ref. [24]. At small $r \le r_c$ distances, the potential $V_p(r) \equiv V_p^{SR}(r)$ corresponds to the electron-correlation potential in an atom and has a form of Eq. (9) from Ref. [24]. At large $r > r_c$ distances, the polarization potential has a well-known asymptotic form $V_p(r) \equiv V_p^{LR}(r) = -\alpha_d/2r^4$, where static dipole polarizability of the indium atom is $\alpha_d = 30.4\ a_0^3$ [4]. These two parts of the polarization potential, $V_p^{SR}(r)$ and $V_p^{LR}(r)$, intersect for the first time at a point $r_c = 4.822\ a_0$.

Spin-orbit interaction of the incident electron with the target atom is taken into account using the potential $V_{so}^{\pm}(r)$ [25] [see also Eq. (5) in Ref. [18]].

The McCarthy-type absorption potential $V_a(r,E)$ [8] (see also different McCarthy potential types in Ref. [9]) has the following general form:

$$V_a(r,E) \equiv VA_i(r,E) = -W_i(E) r^2 \rho_i(r) T_{\mathrm{loc}}^{-2}(r,E), \quad i = 1,2, \tag{3}$$

where $W_i(E)$ is an empirical parameter. We have used the following expression to calculate the local kinetic energy: $T_{\mathrm{loc}} = E - V_s - V_e - V_p$. Note that the McCarthy-type potentials were used in Refs. [8,9] either with total electron density $\rho(r)$ or with highest-occupied electron density $\rho_H(r)$ to study electron scattering by noble-gas atoms. Below we shall demonstrate that in the case of indium atom it is insufficient to use in the McCarthy-type potential only the $5p$- and $5s^2$-subshell densities. Therefore we shall use below two types of absorption potential Eq. (3) (for $i=1$, 2) with two summarized electron densities: $\rho_1 = \rho_{5p} + \rho_{5s}$ and $\rho_2 = \rho_{5p} + \rho_{5s} + \rho_{4d}$, where ρ_{5p}, ρ_{5s}, and ρ_{4d} are electron densities in $5p$-, $5s^2$-, and $4d^{10}$ subshells, respectively. The subshell electron densities ρ_{5p} and ρ_{5s} are expressed by the atomic radial orbitals $\varphi_{n\ell}$: $\rho_{n\ell}(r) = N_{n\ell} |\varphi_{n\ell}(r)|^2$, where $N_{n\ell}$ is the number of electrons in the subshell. The analytical expressions for the φ_{5p} and φ_{5s} orbitals [see formula (B1)] and the summarized ρ_2 density (B2) are presented in Appendix B.

Our calculations for the angular and energy DCS dependences with two VA_i potentials (3) are shown as follows. For 80 and 100 eV, the DCS calculation with VA_2 agrees with the experiment better than that with VA_1. At 40 and 60 eV, the calculation with VA_1 shows better agreement with the experiment. However, when calculating the energy dependence of DCS for angles above 30°, the transition from VA_1 to VA_2 at $E \ge 80$ eV results in a break in the energy dependence of DCS. Therefore, for intermediate energies we suggest using the following generalization of the McCarthy-type absorption potential:

$$VA_3(r,E) = -W_3(E) r^2 [\rho_1(r) + \beta(E) \rho_{4d}(r)] T_{\mathrm{loc}}^{-2}(r,E). \tag{4}$$

The values of $W_i(E)$ parameters in Eq. (3) ($i=1,2$) and Eq. (4) ($i=3$) within the 10–300 eV energy range were determined from the condition of the best agreement of calculated absorption cross sections $\sigma_{\mathrm{abs}}(E)$ with the available experimental inelastic ones $\sigma_{\mathrm{in}}(E) = \sigma_{\mathrm{exc}}(E) + \sigma_{\mathrm{ion}}(E)$. The indium atom excitation cross sections σ_{exc} were taken from experi-

TABLE I. Parameters $W_i(E)$ for the absorption potentials VA_i (3) and (4) and $\beta(E)$ for VA_3. Experimental inelastic cross sections σ_{exc}, σ_{ion}, and $\sigma_{in}=\sigma_{exc}+\sigma_{ion}$ are presented in units 10^{-20} m^2.

E (eV)	σ_{exc} [10]	σ_{ion} [12]	σ_{in}	W_1	W_2	W_3	β
10	4.08	6.19	10.27	0.114	–	0.114	0
20	3.72	11.48	15.20	0.905	–	0.905	0
40	3.27	11.68	14.95	4.75	4.56	4.75	0
60	2.90	10.44	13.34	11.0	10.25	10.75	0.2
70	2.75	9.91	12.66	14.86	13.62	14.2	0.45
80	2.60	9.36	11.96	19.26	17.65	18.11	0.7
100	2.40	8.69	11.09	30.3	27.4	27.68	0.8
200	1.72	6.38	8.10	114.1	95.8	95.8	1.0
300	1.38	4.96[a]	6.34	235.0	188.3	188.3	1.0

[a] σ_{ion} values quoted from [11].

ment [10]. The experimental ionization cross sections σ_{ion} at 10–200 eV were quoted from Ref. [12], while those at 300 eV were quoted from Ref. [11]. The $\sigma_{exc}(E)$, $\sigma_{ion}(E)$, $\sigma_{in}(E)$ cross sections, and obtained values for parameters $W_i(E)$ are presented in Table I. The smoothed energy dependence of $W_3(E)$ parameters is presented in Fig. 1(b). For energies above 300 eV the values of the parameter $W_3(E)$ in Eq. (4) were found by extrapolating its values up to 350 eV [see Fig. 1(b)]. As a result, for $E=350$ eV the value of this parameter is $W_3(E)=254.8$.

The parameter $\beta(E)$ before ρ_{4d} in Eq. (4) is monotonously increasing from 0 up to 1 as the energy increases [see Table I and Fig. 1(c)], and gives a gradual change of the potential shape with energy. As seen from Table I, for $E\leq 40$ eV $\beta=0$ and, hence, $VA_3=VA_1$, whereas for $E\geq 200$ eV the parameter $\beta=1$ and thus, $VA_3=VA_2$. For accounting the absorption effects for the intermediate energies from 60 to 80 eV, a partial influence of the electron density $4d^{10}$ subshell can be used. As seen in Fig. 1(c), in that energy range, $\beta(E)$ increases sharply but continuously.

B. Calculation method

Calculations performed in the SEPASo approximation allow the complex partial phase shifts $\delta_\ell^\pm=\varepsilon_\ell^\pm+i\xi_\ell^\pm$ to be obtained. We use here the phase function method [26,27], which enables the absolute values $\varepsilon_\ell^\pm$ and $\xi_\ell^\pm$ to be calculated as the limits of the phase functions $\varepsilon_\ell^\pm(r)$ and $\eta_\ell^\pm(r)$: $\varepsilon_\ell^\pm=\lim_{r\to\infty}\varepsilon_\ell^\pm(r)$, $\xi_\ell^\pm=-\frac{1}{2}\ln[\lim_{r\to\infty}\eta_\ell^\pm(r)]$. Phase functions $\varepsilon_\ell^\pm(r)$ and $\eta_\ell^\pm(r)$ are found by integrating the system of two coupled first-order nonlinear differential equations [26] [see also Eqs. (10) and (11) in [18]]. To solve numerically this system of equations we used the same method as in Refs. [7,18,19]. At the initial integration points we assumed the absence of absorption, $V_a\cong 0$. For instance, for 300 eV at $r=0.01a_0$, $VA_2=-1.05\times 10^{-8}$ (a.u.), which is negligibly small as compared to the value of the real part of $V_{opt}^-(1)$: $V_R^-=-4.08\times 10^3$ (a.u.). Therefore, for the small radial distances r, where $V_a\cong 0$ and $\eta_\ell^\pm=1$, the solution of the system of equations for the phase functions is reduced to integrating only the single equation for $\varepsilon_\ell^\pm(r)$ (see Ref. [18], and references therein).

The number of calculated pairs of phase shifts δ_ℓ^+ and δ_ℓ^-, similar to Ref. [18], was different in dependence with the collision energy. So, for 10 eV we put them equal, $\delta_\ell^+=\delta_\ell^-$, starting from $\ell=4$, while for 300 eV—starting from $\ell=20$. For such ℓ, starting from which the imaginary part of the phase shift is $\xi_\ell\leq 10^{-4}$ rad, whereas its real part is $\varepsilon_\ell\leq 0.01$ rad, we began to compare the value of ε_ℓ with the asymptotic values of the phase shift δ_ℓ^{as} determined by known formula [28] [see also Eq. (56) in Ref. [19]]. When the difference $|\varepsilon_\ell-\delta_\ell^{as}|$ became minimal, i.e., at $\ell=L_1$, we stopped calculating δ_ℓ by the phase equations and assumed for $\ell>L_1$ that $\varepsilon_\ell=\delta_\ell^{as}$ and $\xi_\ell=0$. For example, for 10 eV we obtained $L_1=14$, where $\delta_{14}(10)=2.83\times 10^{-3}+i9.04\times 10^{-5}$ (rad), while for 300 eV—$L_1=50$, where $\delta_{50}(300)=1.92\times 10^{-3}+i8.59\times 10^{-5}$ (rad).

Using calculated phase shifts $\delta_\ell^\pm(E)$ we, similarly to Ref. [7], obtained the direct scattering amplitude $f(\theta)$, the spin-flip scattering amplitude $g(\theta)$, the elastic differential cross section $d\sigma(\theta)/d\Omega$, the integral elastic scattering $\sigma_{el}(E)$, momentum transfer $\sigma_m(E)$, and viscosity $\sigma_v(E)$ cross sections, but with the allowance the phase shifts complexity. The absorption cross section $\sigma_{abs}(E)$ describing the electron excitation and ionization processes is calculated as in Ref. [19]. The total scattering cross section is found as the sum $\sigma_{tot}=\sigma_{el}+\sigma_{abs}$.

IV. RESULTS AND DISCUSSIONS

The relative values of experimental DCSs are normalized at 20° to the SEPASo theory (with VA_3) and presented in Table II. The comparison of the present experimental results with the present theoretical DCSs calculated in SEPSo and SEPASo approximations are presented in Figs. 2 and 3.

DCSs measured experimentally and calculated in two approximations at 10 and 20 eV are shown in Figs. 2(a) and 2(b). Note that for these energies, calculations with VA_1 and VA_3 [see $W_i(E)$ and β in Table I] coincide. As seen from Figs. 2 and 3, the SEPSo calculation for all energies, except for 10 eV, reproduces the shape of the angular dependence of experimental cross sections, the number of minima, and their angular positions. For 10 eV in theoretical calculations, as well as in the experiment, one minimum was obtained, but at

TABLE II. Experimental differential elastic cross sections, in units of 10^{-20} m^2 sr^{-1}, for electron scattering by the indium atom normalized at 20° to the SEPASo (with VA_3). The numbers in parentheses are normalized relative errors.

Angle (deg)	Electron energy (eV)					
	10	20	40	60	80	100
10	62.7(4.1)	45.6(2.9)	34.6(2.2)	25.1(1.6)	19.1(1.2)	13.25(84)
20	17.8(1.2)	8.26(51)	3.66(23)	2.41(16)	1.78(11)	1.429(89)
30	4.91(33)	1.174(74)	0.540(42)	0.834(60)	0.824(52)	0.734(47)
40	1.143(93)	0.116(10)	0.266(25)	0.395(34)	0.395(26)	0.327(22)
50	0.236(38)	0.071(10)	0.337(30)	0.177(22)	0.0931(77)	0.0632(63)
60	0.110(27)	0.1031(91)	0.425(35)	0.096(16)	0.0151(28)	0.0095(26)
70	0.070(15)	0.0876(82)	0.252(25)	0.055(13)	0.0497(51)	0.0668(66)
80	0.048(13)	0.0457(56)	0.073(13)	0.032(11)	0.0781(69)	0.1000(86)
90	0.048(15)	0.0199(39)	0.0193(85)	0.0636(96)	0.0753(67)	0.0828(76)
100	0.031(14)	0.0095(31)	0.20(3)	0.117(14)	0.0607(58)	0.0289(41)
110	0.029(15)	0.0143(35)	0.330(30)	0.189(19)	0.0512(52)	0.0144(31)
120	0.074(17)	0.0211(39)	0.362(32)	0.256(26)	0.0670(61)	0.0132(29)
130	0.118(20)	0.0192(37)	0.227(23)	0.180(21)	0.0343(40)	0.0143(30)
140	0.167(21)	0.0589(63)	0.0234(85)	0.037(10)	0.0049(18)	0.0081(24)
150	0.307(30)	0.189(14)	0.093(14)	0.088(13)	0.0636(58)	0.0464(51)

86°, that is about 20° shifted toward the lower angles than in the experimental DCS. Account of the absorption potential does not change the shape of DCS but only decreases its values at intermediate and large scattering angles. Thus, to describe reliably the DCSs at low energies, in particular, at 10 eV, one needs to modify first the real part $V_R(r,E)$ (2) of the optical potential, mainly the polarization and exchange potentials.

Figure 1(a) presents the results of two different approximations of the total radial electron densities of indium $\rho(r)$ using Eq. (A1) and from Ref. [[21], Eq. (12)]. Using these approximations we presented theoretical and experimental DCSs at 20 eV in Fig. 2(b). The angular positions of both DCS minima and local maxima with the $\rho(r)$ density taken from Ref. [21] are shifted by 5°–10° toward the lower angles with respect to the present experimental data and our SEPSo calculation with $\rho(r)$ from Eq. (A1). Note also that DCS with $\rho(r)$ taken from Ref. [21] at low angles (0°–20°) is 1.2–1.6 times less and at 180° is 1.2 times larger than the present calculation.

The absorption potential VA_3 with $W_3(E)$ and $\beta(E)$ from Table I is used in systematic calculations of both differential and integral scattering cross sections at intermediate energies. Above we mentioned that in the SEPASo calculation the DCS could be calculated at the 10–60 eV energies using the absorption potential VA_1 (3) (two subshells—$5p$ and $5s^2$ being taken into account), while for the energies above 80 eV—with VA_2 (total account of the $4d^{10}$ subshell is added). At the same time, to obtain continuous DCS energy dependence in the 60–80 eV energy interval we had to use the VA_3 potential (4), which allowed us to increase gradually the contribution of the $4d^{10}$ subshell with energy. In Figs. 2(d) and 3(a)–3(c), DCSs calculated using several approximations (with and without the absorption) are compared with the experimental data at 40, 60, 80, and 100 eV.

For 40 eV calculations using VA_1 and VA_3 coincide. It is seen that for 40 and 60 eV it is sufficient to take into account in the absorption potential the densities ρ_{5p} and ρ_{5s} (the VA_1 calculation). At 80 and 100 eV the inclusion into the absorption potential of the density ρ_{4d} (the VA_2 calculation) gives a better agreement with the experimental data at intermediate and large scattering angles as compared to calculation using VA_1.

At the same time, as seen from Fig. 3(a), calculation using VA_3 (β=0.2) agrees for 60 eV with experiment at 60°–120° better than that one using VA_1 (β=0). For 80 eV [see Fig. 3(b)] at 120°–130°, and for 100 eV [see Fig. 3(c)] at 110°–120° the calculation using VA_3 (β=0.7 and β=0.8, respectively) agrees with experiment better than that one using VA_2. Thus, the comparison of our calculations with the present experiment allowed more smooth energy dependence of parameter $\beta(E)$ to be obtained [see Fig. 1(c)] as compared to the case when this parameter is strictly equal to 0 at 60 eV and to 1 at 80 and 100 eV. As seen from Fig. 3, the DCSs for 60, 80, and 200 eV have the deepest minima.

In Fig. 4, the angular positions of the DCS minima calculated both with and without absorption are shown. In the 20–48 eV energy interval, DCS reveals three minima: between 50 and 100 eV—two minima, and above 102 eV—again three minima. Except for a small energy interval from 17 to 21 eV at 107°–121°, in general, two calculations agree well with each other. From the comparison of theory with the experiment it could be concluded that beginning from 20 eV the tendencies in changes of angular positions of minima coincide. The largest differences between the SEPASo calculations and the experimental data have been obtained at 40 eV for the first minimum (min1) and the second one (min2), and at 100 eV for (min2) and (min3). In Fig. 4, the angular positions of the six deepest minima, so-called critical minima (see, e.g., Ref. [29]), calculated in SEPASo and the seven

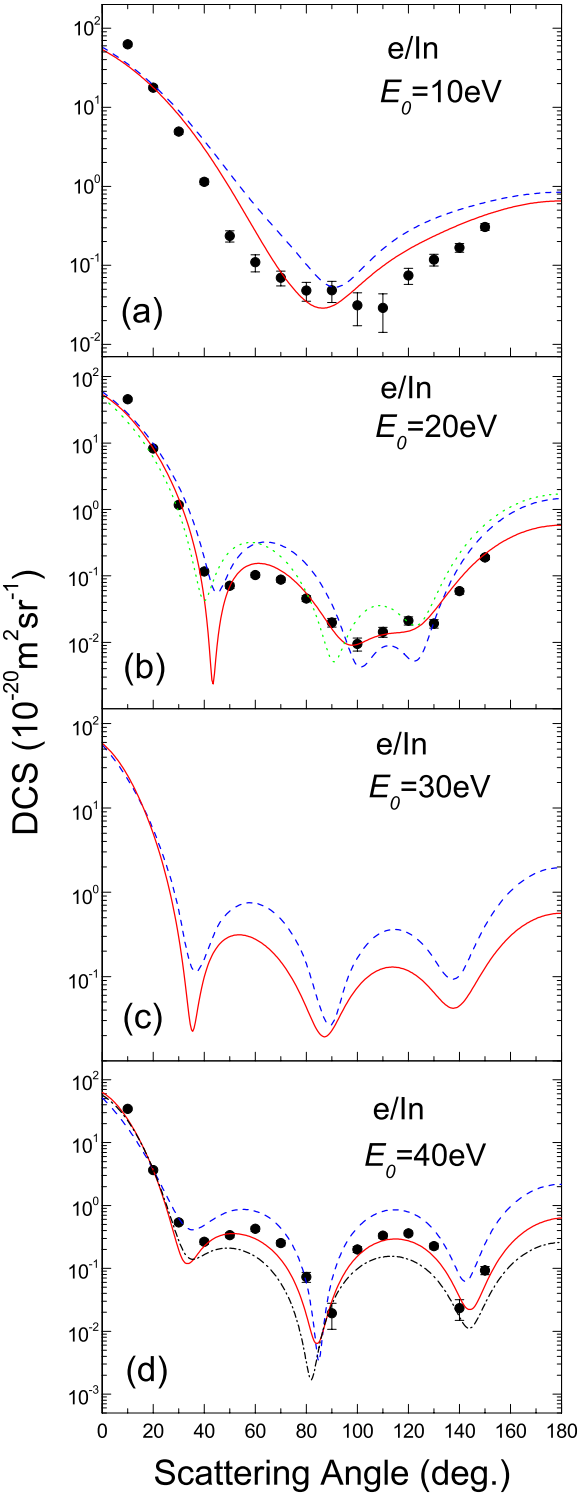

FIG. 2. (Color online) Differential elastic-electron–indium-atom scattering cross sections (in units of 10^{-20} m^2 sr^{-1}) at (a) 10 eV, (b) 20 eV, (c) 30 eV, and (d) 40 eV. The dashed line shows the results obtained by SEPSo theory (without absorption). The solid line shows the results obtained by the SEPASo theory (Eq. (1) with absorption potential VA_3 [Eq. (4)]). The dotted line at 20 eV shows DCSs calculated by the SEPSo theory with $\rho(r)$ from [21]. The dash-dotted line at 40 eV shows the results obtained by the SEPASo with potential VA_2 [Eq. (3)]. Circles with error bars represent the experimental results normalized at 20° to the SEPASo calculation (with VA_3).

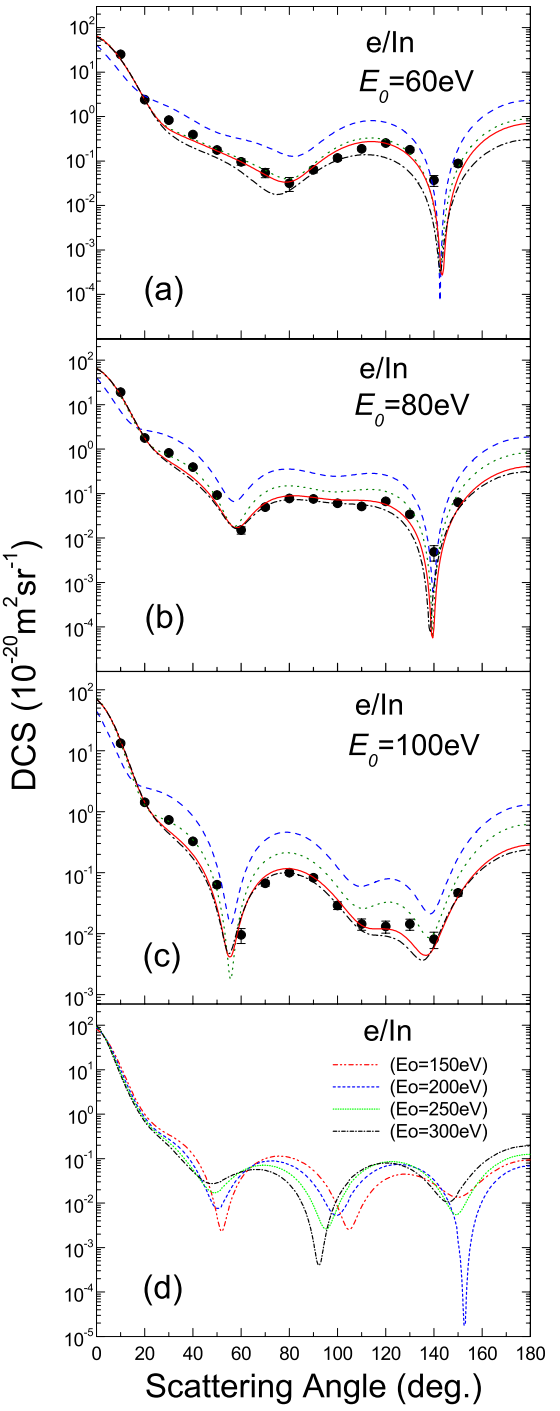

FIG. 3. (Color online) Differential elastic-electron–indium-atom scattering cross sections (in units of 10^{-20} m^2 sr^{-1}) at (a) 60 eV, (b) 80 eV, (c) 100 eV impact energies. The dashed line shows the results obtained by SEPSo theory (without absorption). The results of SEPASo theory [with absorption, Eq. (1)] are represented with potentials VA_1 [Eq. (3)], VA_2 [Eq. (3)], and VA_3 [Eq. (4)]. The dotted line, dash-dotted line, and the solid line denotes, respectively, VA_1, VA_2, and VA_3 potentials of the SEPASo theory. Circles with error bars represent the experimental results normalized at 20° to the SEPASo calculation (with VA_3). The results in (d) are represented by SEPASo theory only. The dash-dot-dotted (red), short-dashed (blue), short-dotted (green), and short-dash-dotted (black) lines denote, respectively, 150 eV, 200 eV, 250 eV, and 300 eV impact energies.

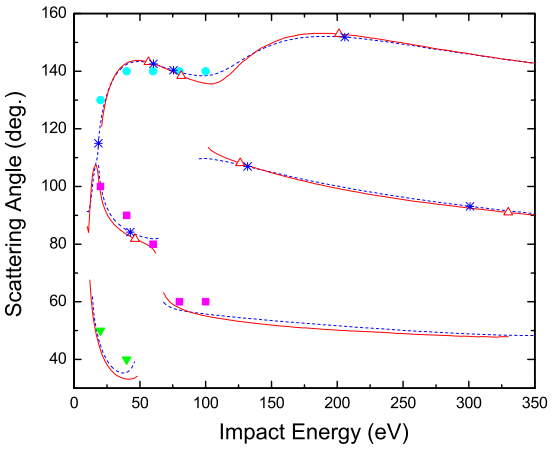

FIG. 4. (Color online) Energy dependence of angular positions of minima in the differential elastic-electron–indium-atom cross sections. The dashed and solid lines show the results obtained by SEPSo and SEPASo theories, respectively. The stars and open triangles are critical minima calculated without and with absorption, respectively. The down triangles, rectangles, and circles are the first, second, and third experimentally obtained minima, respectively.

deepest minima calculated in the SEPSo approximation are presented. The energy positions of five critical minima found in two approximations agree well with each other. As seen from Fig. 4 and Table III, the SEPASo calculation gives no minimum at ~18 eV. Figures 2(b) show that the calculation with absorption at 20 eV does not provide the third minimum at $\theta > 110°$. In the SEPSo calculation, we found a critical minimum at 300.9 eV. The SEPASo calculations indicated that this high-energy minimum lies above 300 eV.

For indium atom in the SEPASo approximation (see Fig. 4) we obtained six minima between 10 and 350 eV. Taking into account the high-energy critical minimum at 635.0 eV and 131.27° found in the SEPSo approximation, the presence of seven critical DCS minima for indium atom may be assumed. It is of certain interest the further investigation of the variation of the critical minima number in DCS with filling the valence subshell in atoms belonging to the $5p$ series. The last atom of the $5p$ series, xenon, has ten critical minima in the 50–780 eV energy range [30].

TABLE III. Energies E_c (eV) and angles θ_c (deg) of the critical minima in DCS for elastic-electron scattering by indium atoms calculated in the SEPSo [without absorption, Eq. (2)] and the SEPASo [Eq. (1) with VA_3 (4)] approximations.

SEPSo		SEPASo	
E_c (eV)	θ_c (deg)	E_c (eV)	θ_c (deg)
18.5	114.98		
42.7	84.18	46.3	81.84
60.4	142.50	56.6	143.16
75.5	140.33	81.5	138.37
131.9	106.95	126.2	108.13
205.7	151.82	201.4	152.88
300.9	93.13	330.0	91.01

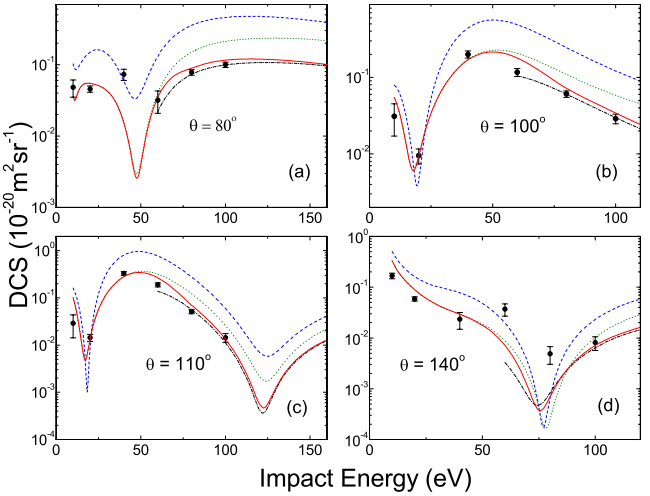

FIG. 5. (Color online) Energy dependence of differential cross sections (in units of 10^{-20} m^2 sr^{-1}) for the elastic-electron scattering by the indium atom at fixed angle (a) 80°, (b) 100°, (c) 110°, and (d) 140°. Notations are the same as for Fig. 3.

The dependence of OP on the collision energy is defined first of all by the energy dependence of the absorption potential [see Eqs. (1)–(4)]. The absence of any adjustable parameter in $V_R(r,E)$ (2) gives fundamental significance to the SEPSo calculations, especially in structures of the energy dependence of DCSs within a wide energy range. The most interest is in the comparison of experiment and theory for the energies and angles in the vicinity of the critical minima (see Table III). Figures 5(a)–5(d) illustrate the energy dependences of DCS measured experimentally and DCS calculated in the previously described four approximations [see Figs. 3(a)–3(c) for intermediate scattering angles]. Figure 5 shows that even a slight variation of scattering angles (80°–140°) results in the qualitatively different energy dependence of DCSs.

As seen from Figs. 2 and 3, at 20° the SEPSo and SEPASo calculations almost coincide for 10, 20, 40, and 60 eV, and for 80 and 100 eV the SEPSo calculation exceeds the SEPASo calculation only 1.5 and 1.8 times, respectively. As for the intermediate scattering angles, the SEPSo calculation exceeds, as a rule, the SEPASo calculation with VA_3 by 3–4 times. The only exception are the ratios of DCS values at certain minima—e.g., for 100° and 110° [Figs. 5(b) and 5(c)] at ~20 eV and for 140° [Fig. 5(d)] at ~76 eV.

For 80° [Fig. 5(a)] the SEPASo calculation with VA_3 agrees, in general, with experiment except for 40 eV. As seen in Fig. 2(d), for 40 eV the experimental DCS has a minimum at 90°, not at ~80° as the calculated DCSs show.

For 100° and 110° [Figs. 5(b) and 5(c)], the energy dependences of DCS reveal a deep minimum at ~20 eV. Figure 2(b) shows that at these angles the SEPSo calculation lies slightly below the experimental data and the SEPASo calculation. For $E \geq 40$ eV all the SEPASo calculations agree with experiment noticeably better than the SEPSo calculation. In turn, for $E \geq 60$ eV calculations with VA_2 and VA_3 agree with experiment better than those with VA_1. For 110° [Fig. 5(c)] the minimum at ~120 eV is observed in all four approximations.

For 140° [Fig. 5(d)] the SEPASo calculation with VA_3 agrees well with experiment except for 60 and 80 eV. As follows from Figs. 3(a) and 3(b), the experimental DCSs also have the high-angle minimum at 140°. However, at this minimum the experimental cross sections are several orders of magnitude larger than the theoretical ones.

A comparison of theoretical calculations with experiment in Figs. 5(a)–5(d) indicates the necessity of a more thorough experimental study of DCS close to the intermediate-angle minimum (80°–100°) for 20–60 eV and the high-angle minimum at 140° for the energies from the 60–100 eV interval. Present experimental study could not cover these minima because of the low signal. In general, as Figs. 3–5 show, positions of minima in the angular and energy dependences of DCSs obtained in SEPASo and SEPSo calculations agree well with each other. The SEPASo calculation with VA_1 also is in a good agreement with VA_2, but only the use of VA_3 gives the continuous energy dependence of DCSs (see Fig. 5).

In Fig. 6 and Table IV, the integral elastic $\sigma_{el}(E)$, momentum-transfer $\sigma_m(E)$, and viscosity $\sigma_v(E)$ cross sections measured experimentally and calculated using the SEPSo and the SEPASo [with VA_3 (4)] approximations are compared. As seen in Fig. 6, the theoretical cross sections provide the shape of the energy dependence of the experimental integral cross sections. The SEPASo σ_{el} calculation [see Fig. 6(a)] is in good agreement with the experiment at 10, 60, and 80 eV. At 20 and 40 eV the calculation with absorption lies slightly lower, and at 100 eV—higher than experiment.

Absorption cross sections σ_{abs} calculated in SEPASo approximation using the potential VA_3 (4) with the parameters $W_3(E)$ and $\beta(E)$, which were obtained from smooth energy dependences [see Figs. 1(b) and 1(c)] are presented in Table IV. The σ_{abs} values are in a good agreement with the earlier obtained experimental inelastic cross sections σ_{in} [10–12] (see Table I). Some difference between σ_{abs} and experimental σ_{in} was obtained for 70 and 80 eV. However, this difference does not exceed the value 7×10^{-22} m^2.

As seen in Table IV, the absorption cross sections σ_{abs} beginning from 15 eV up to 300 eV, exceed σ_{el}. At the maximum at 25 eV and at 300 eV σ_{abs} contributes more than 60% to the total cross section σ_{tot}. So large a contribution of the absorption cross section to the σ_{tot} is due to the relatively large ionization cross section σ_{ion} of the indium atom [11,12] (see also Table I). As seen from Tables I and IV, the experimental σ_{ion} exceeds even at 300 eV the SEPASo σ_{el} (by 1.3 times). It testifies the importance of the absorption effect accounts at the different integral cross section calculations for electron scattering by indium atom. Particularly, it is well seen on the example of the σ_m and σ_v cross-section values [Figs. 6(b) and 6(c)]. The SEPASo calculations of these cross sections agree well with the present experiment. Both theory and experiment reveal minima at $W_3(E)$ and maxima at ~40–50 eV. As seen in Table IV, calculations with absorption the σ_m and σ_v cross sections have minima at 22 eV and maxima at 48 and 45 eV, respectively.

V. CONCLUSIONS

Differential cross sections for the elastic-electron scattering by indium atom in the intermediate energy region were studied for the first time both experimentally and theoretically. Experimental investigation of elastic-electron scattering by In atoms was performed using crossed beam technique for the energy range from 10 to 100 eV. The measurements were performed for a large angular range from 10° up to 150° and with a good angular resolution of 1.5°. The scattered electron intensity was measured as a function of the scattering angle. Angular distributions were multiplied by effective length correction factors in order to obtain relative DCS. These DCSs normalized at 20° to the present theoretical calculations with absorption allowance (SEPASo) and extrapolated to 0° and 180° were used to obtain the experimental integral elastic, momentum-transfer, and viscosity cross sections.

Theoretical calculations were carried out using a model phenomenological complex potential with the inclusion of spin-orbit interaction. The static potential, the total and subshell electron densities of the In atom were calculated within

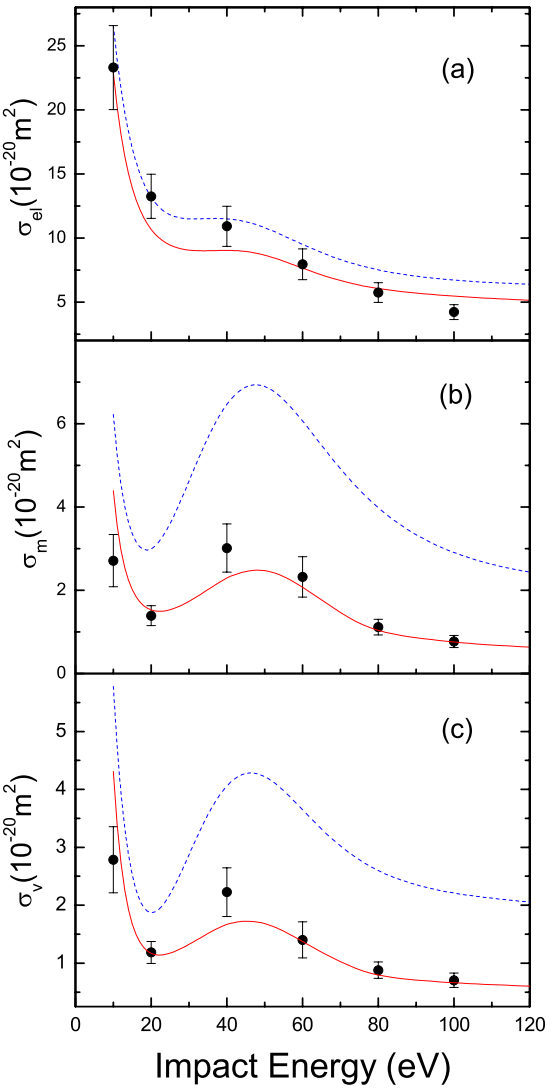

FIG. 6. (Color online) Integral elastic σ_{el} (a), momentum-transfer σ_m (b), and viscosity σ_v (c) cross sections (in units of 10^{-20} m^2) for elastic-electron scattering by indium atoms. Notations are the same as for Fig. 3.

TABLE IV. Calculated and measured values of the integral elastic (σ_{el}), absorption (σ_{abs}), total (σ_{tot}), momentum-transfer (σ_m), and viscosity (σ_v) cross sections (in units of 10^{-20} m^2) for electron scattering by indium atoms. SEPSo corresponds to the use of a real potential (2), SEPASo to the use of a complex potential (1) with the absorption potential VA_3 (4). The experimental absolute errors are indicated in parentheses.

Energy (eV)	σ_{el}			σ_{abs}	σ_{tot}	σ_m			σ_v		
	SEPSo	SEPASo	Experiment	SEPASo	SEPASo	SEPSo	SEPASo	Experiment	SEPSo	SEPASo	Experiment
10	26.61	22.91	23.3(3.3)	10.29	33.20	6.224	4.395	2.71(0.63)	5.779	4.310	2.79(0.57)
15	17.02	13.91		13.93	27.84	3.357	2.016		2.523	1.676	
20	13.18	10.67	13.3(1.7)	15.22	25.89	2.995	1.528	1.39(0.24)	1.870	1.171	1.18(0.19)
22	12.43	10.03		15.44	25.47	3.159	1.494		1.925	1.140	
25	11.81	9.445		15.60	25.05	3.603	1.532		2.191	1.172	
30	11.50	9.055		15.56	24.62	4.624	1.734		2.872	1.325	
35	11.52	9.005		15.32	24.33	5.667	2.015		3.563	1.511	
40	11.50	9.041	10.9(1.6)	14.96	24.00	6.465	2.299	3.02(0.58)	4.059	1.671	2.23(0.42)
45	11.27	8.948		14.64	23.59	6.883	2.451		4.274	1.724	
50	10.81	8.661		14.21	22.87	6.896	2.471		4.220	1.683	
55	10.18	8.192		13.75	21.94	6.579	2.330		3.977	1.553	
60	9.501	7.648	7.95(1.20)	13.32	20.97	6.065	2.071	2.32(0.48)	3.648	1.375	1.40(0.31)
70	8.320	6.681		12.59	19.27	4.918	1.469		3.023	1.027	
80	7.517	6.053	5.74 (0.77)	12.03	18.08	3.983	1.035	1.12(0.19)	2.600	0.7955	0.879(0.141)
90	7.021	5.705		11.51	17.22	3.334	0.8615		2.353	0.7094	
100	6.718	5.465	4.22(0.58)	11.09	16.56	2.906	0.7575	0.770(0.148)	2.211	0.6621	0.705(0.125)
150	6.120	4.794		9.515	14.31	2.141	0.5760		1.881	0.5569	
200	5.725	4.359		8.104	12.46	1.923	0.5693		1.570	0.4984	
250	5.325	4.059		7.025	11.08	1.758	0.6028		1.285	0.4592	
300	4.953	3.807		6.339	10.15	1.602	0.6045		1.064	0.4079	

the framework of a local relativistic approximation of the density functional theory with the exclusion of electron self-action energy. The analytical expressions with the optimal number of parameters were suggested for these values. Both exchange and parameter-free polarization potentials were expressed via the total electron density, while the absorption potential was expressed via the subshell electron densities. This allows us to consider the calculations of the scattering characteristics to be carried out using a single approach.

The use of the McCarthy-type absorption potential allowed the role of the valence $5p$, and subvalence $5s^2$ and $4d^{10}$ subshells to be studied to describe the absorption effects in the electron scattering by the indium atom. Just a combined experimental and theoretical study has shown the necessity to take into account, beginning from 80 eV, besides the $5s^2$ and $5p$ subshells, the $4d^{10}$ subshells as well. To obtain the continuous energy dependence of DCS in the 60–80 eV range we suggested generalizing the McCarthy-type absorption potential in a form of the potential VA_3 (4). It gave the possibility to realize a partial account of multielectron subvalence subshell ($4d^{10}$ in our case) depending on the collision energy.

Two methods of absorption effect accounted in the above scattering were suggested. The first of them relates to the use of the potential VA_1 with the electron density of the $5p$ and $5s^2$ subshells being taken into account for the energies below 60 eV. Above 80 eV the VA_2 potential was used with the allowance made for the electron density of the $4d^{10}$ subshell. The empirical parameters $W_1(E)$ and $W_2(E)$ for these potentials were determined using the experimental integral excitation and ionization cross sections. The second method uses at any energy the VA_3 potential with the possibility to take partially into account the absorption by the $4d^{10}$ subshell by introducing the factor $\beta(E) \in [0,1]$, which is determined from the best agreement of theoretical and experimental DCS behaviors above 90°. The values of the $W_3(E)$ parameter, as well as W_1 and W_2, can be found using the same integral inelastic scattering cross sections. Thus, the VA_3 potential can be applied to obtain systematic DCS data, in particular, those on their minima within a wide intermediate energy range.

Comparison of the SEPSo and SEPASo approximations allows one to state that the SEPSo calculation with no use of adjustable parameters can be applied, at least, to predict qualitatively the behavior of both the angular and the energy dependences of DCS within a wide intermediate energy range. As regards the DCS minima, a good agreement of their energy positions obtained in these two approximations enables one to conclude that the use of the energy-dependent phenomenological parameter $W(E)$ in the absorption potential resulted in the change of the DCS value only, not of its shape. Therefore, it may be assumed that the absorption potential is a correction to $V_R(r,E)$ (2)—the main force part of the optical potential (1).

ACKNOWLEDGMENTS

This work has been carried out in part within the project No. 141011 financed by Ministry of Science of Republic of Serbia.

APPENDIX A: PARAMETERS FOR ANALYTICAL EXPRESSIONS FOR THE TOTAL ELECTRON DENSITY $\rho(r)$ AND STATIC POTENTIAL $V_s(r)$

The electron density $\rho(r)$ and static potential $V_s(r)$ are calculated using analytical expressions from [20]

$$\rho(r) = \frac{Z}{4\pi r}\left[\sum_{i=1}^{n} {}^{a}\gamma_i {}^{a}\lambda_i^2 \exp(-{}^{a}\lambda_i r) + \sum_{j=1}^{m} {}^{b}\gamma_j {}^{b}\lambda_j ({}^{b}\lambda_j r - 2)\exp(-{}^{b}\lambda_j r)\right], \quad \text{(A1)}$$

$$V_s(r) = -\frac{Z}{r}\left[\sum_{i=1}^{n} {}^{a}\gamma_i \exp(-{}^{a}\lambda_i r) + r\sum_{j=1}^{m} {}^{b}\gamma_j \exp(-{}^{b}\lambda_j r)\right], \quad \text{(A2)}$$

where Z is the nuclear charge of the target atom. In Eqs. (A1) and (A2) summation is taken up to $n=4$ and $m=5$. The parameters γ and λ have the following values: ${}^{a}\gamma_1=4.484\ 39$, ${}^{a}\gamma_2=-1.158\ 54$, ${}^{a}\gamma_3=1-{}^{a}\gamma_1-{}^{a}\gamma_2-{}^{a}\gamma_4$, and ${}^{a}\gamma_4=-1.649\ 75$ are dimensionless; ${}^{a}\lambda_1=4.790\ 69$, ${}^{a}\lambda_2=14.271\ 66$, ${}^{a}\lambda_3=76.777\ 16$, ${}^{a}\lambda_4=21.0$, ${}^{b}\lambda_1=7.8125$, ${}^{b}\lambda_2=18.534\ 55$, ${}^{b}\lambda_3=55.495\ 95$, ${}^{b}\lambda_4=2.089\ 31$, ${}^{b}\lambda_5=1.135$, ${}^{b}\gamma_1=-25.0935$, ${}^{b}\gamma_2=-33.591\ 97$, ${}^{b}\gamma_3=-29.311\ 64$, ${}^{b}\gamma_4=0.3296$, and ${}^{b}\gamma_5=0.039\ 06$—in a_0^{-1} units; a_0 is the first Bohr radius of hydrogen atom.

APPENDIX B: ANALYTICAL EXPRESSIONS AND PARAMETERS FOR THE $\varphi_{5p}(r)$ AND $\varphi_{5s}(r)$ ORBITALS AND SUMMARIZED DENSITY $\rho_2(r)$

The following expression was used to approximate the $n\ell$ orbitals:

$$\varphi_{n\ell}(r) = \sum_{j=1}^{K_{n\ell}} M_i r^{M_{i+1}} \exp(-M_{i+2} r), \quad \text{(B1)}$$

where $i=3j-2$. For the $5p$ subshell $N_{5p}=1$, $K_{5p}=5$ and the parameters have the following values: $M_1=-94.345\ 81$, $M_2=1.9$, $M_3=9.910\ 33$, $M_4=114.813\ 73$, $M_5=1.488\ 05$, $M_6=31.436\ 14$, $M_7=1.199\ 54$, $M_8=0.3$, $M_9=2.343\ 67$, $M_{10}=-0.166\ 73$, $M_{11}=1.3$, $M_{12}=0.918\ 31$, $M_{13}=-0.020\ 72$, $M_{14}=0.1595$, and $M_{15}=0.301\ 82$.

For the $5s$ subshell $N_{5s}=2$, $K_{5s}=6$ and the parameters are $M_1=163.976\ 47$, $M_2=1.652\ 17$, $M_3=8.311\ 71$, $M_4=-300$, $M_5=2.898\ 92$, $M_6=9.8807$, $M_7=-3.865\ 41$, $M_8=0.086\ 62$, $M_9=2.717\ 83$, $M_{10}=0.292\ 82$, $M_{11}=0.959\ 39$, $M_{12}=1.067\ 93$, $M_{13}=0.264\ 29$, $M_{14}=-0.214\ 78$, $M_{15}=0.784\ 12$, $M_{16}=7.202\ 99$, $M_{17}=0.043\ 82$, and $M_{18}=36.694\ 36$.

The following analytical expression was used to approximate the summarized density ρ_2:

$$\rho_2(r) = \left[\sum_{j=1}^{6} G_i r^{G_{i+1}} \exp(-G_{i+2} r)\right]^2, \quad \text{(B2)}$$

where $i=3j-2$, and the parameters are $G_1=-80.207\ 16$, $G_2=2.670\ 36$, $G_3=5.319\ 01$, $G_4=99.870\ 18$, $G_5=1.1484$, $G_6=7.708\ 77$, $G_7=-1.8119$, $G_8=0.529\ 15$, $G_9=1.5$, $G_{10}=-0.2491$, $G_{11}=0.575\ 27$, $G_{12}=0.668\ 89$, $G_{13}=153$, $G_{14}=0.52$, $G_{15}=139.33$, $G_{16}=-12.5$, $G_{17}=0.774\ 23$, and $G_{18}=25.83$.

[1] S. Djeniže, A. Srećković, and S. Bukvić, Spectrochim. Acta, Part B **61**, 588 (2006).

[2] N. Vitas, I. Vince, M. Lugaro, O. Andriyenko, M. Gosic, and R. J. Rutten, Mon. Not. R. Astron. Soc. **384**, 370 (2008).

[3] Th. Becker J. v. Zanthier, A. Yu. Nevsky, Ch. Schwedes, M. N. Skvortsov, H. Walther and E. Peik, Phys. Rev. A **63**, 051802 (2001).

[4] T. M. Miller and B. Bederson, *Advances in Atomic and Molecular Physics*, edited by D. R. Bates and B. Bederson (Academic, New York, 1977), Vol. 13, pp. 1–55.

[5] S. Milisavljevic, D. Sevic, R. K. Chauhan, V. Pejcev, D. M. Filipovic, R. Srivastava, and B. P. Marinkovic, J. Phys. B **38**, 2371 (2005).

[6] B. Predojević, D. Šević, V. Pejčev, B. P. Marinković, and D. M. Filipović, J. Phys. B **38**, 1329 (2005).

[7] V. I. Kelemen, M. M. Dovhanych, and E. Yu. Remeta,J. Phys. B **41**, 035204 (2008).

[8] I. E. McCarthy, C. J. Noble, B. A. Philips, and A. D. Turnbull, Phys. Rev. A **15**, 2173 (1977).

[9] G. Staszewska, D. W. Schwenke, and D. G. Truhlar, Phys. Rev. A **29**, 3078 (1984).

[10] L. L. Shimon and E. I. Nepiipov, Ukr. Fiz. Zh. (Russ. Ed.) **19**, 626 (1974).

[11] L. L. Shimon, E. I. Nepiipov, and I. P. Zapesochnyi, Zh. Tekh. Fiz. **45**, 688 (1975); Sov. Phys. Tech. Phys. **20**, 434 (1975).

[12] R. S. Freund, R. C. Wetzel, R. J. Shul, and T. R. Hayes, Phys. Rev. A **41**, 3575 (1990).

[13] B. P. Marinković, V. Pejčev, D. Šević, M. S. Rabasović, D.M. Filipović, V. I. Kelemen, M. M. Dovhanych, and E. Yu. Remeta, in *Proceedings of the 25th International Conference on Photonic, Electronic and Atomic Collisions, Freiburg, 2007*, edited by J. Anton, R. Moshammer, C. D. Schröter, and J. Ullrich (Max-Planck-Institut für Kemphysik, Heidelberg, 2007), p. Tu046.

[14] D. M. Filipović, B. Predojević, D. Šević, V. Pejčev, B. P. Marinković, R. Srivastava, and A. D. Stauffer, Int. J. Mass. Spectrom. **251**, 66 (2006).

[15] S. Milisavljević, M. S. Rabasović, D. Šević, V. Pejčev, D. M. Filipović, Lalita Sharma, Rajesh Srivastava, A. D. Stauffer, and B. P. Marinković, Phys. Rev. A **75**, 052713 (2007).

[16] B. P. Marinković, V. Pejčev, D. M. Filipović, D. Šević, S. Milisavljević, and B. Predojević, Radiat. Phys. Chem. **76**, 455

(2007).
[17] R. T. Brinkmann and S. Trajmar, J. Phys. E **14**, 245 (1981).
[18] A. R. Milosavljevic,V. I. Kelemen, D. M. Filipovic, S. M. Kazakov, V. Pejcev, D. Sevic, and B. P. Marinkovic, J. Phys. B **38**, 2195 (2005).
[19] V. I. Kelemen, E. Yu. Remeta, and E. P. Sabad, J. Phys. B **28**, 1527 (1995).
[20] T. G. Strand and R. A. Bonham, J. Chem. Phys. **40**, 1686 (1964).
[21] F. Salvat, J. D. Martínez, R. Mayol, and J. Parellada, Phys. Rev. A **36**, 467 (1987).
[22] S. Sur and A. S. Ghosh, Int. J. Quantum Chem. **57B**, 67 (1983).
[23] A. A. Radtsig and B. M. Smirnov, *Reference Data on Atoms, Molecules, and Ions* (Énergoatomizdat, Moscow, 1986/ Springer-Verlag, Berlin, 1985).
[24] N. T. Padial and D. W. Norcross, Phys. Rev. A **29**, 1742 (1984).
[25] R. Cowan, *The Theory of Atomic Structure and Spectra* (University of California Press, Berkeley, 1981).
[26] F. Calogero, *Variable Phase Approach to Potential Scattering* (Academic, New York, 1967; Mir, Moscow, 1972).
[27] V. V. Babikov, *Variable Phase Method in Quantum Mechanics* (Nauka, Moscow, 1988).
[28] P. G. Burke, *Potential Scattering in Atomic Physics* (Plenum, New York, 1977).
[29] R. Panajotovic, D. Filipovic, B. P. Marinković, V. Pejcev, M. Kurepa, and L. Vuskovic, J. Phys. B **30**, 5877 (1997).
[30] J. Kessler, J. Liedtke, and C. B. Lukas, in *Proceedings of the International Summer School and Symposium on the Physics of Ionized Gases, Dubrovnik, 1976*, edited by B. Navinšek (J. Stefan Institute, Ljubljana, 1976), p. 61.